

**Spin fluctuations in the ultranodal superconducting state of Fe(Se,S)**Yifu Cao<sup>1,\*</sup>, Chandan Setty<sup>2</sup>, Andreas Kreisel<sup>3</sup>, Laura Fanfarillo<sup>1,4</sup> and P. J. Hirschfeld<sup>1</sup><sup>1</sup>*Department of Physics, University of Florida, Gainesville, Florida 32603, USA*<sup>2</sup>*Department of Physics and Astronomy, Rice Center for Quantum Materials, Rice University, Houston, Texas 77005, USA*<sup>3</sup>*Niels Bohr Institute, University of Copenhagen, Jagtvej 155, DK-2200, Copenhagen, Denmark*<sup>4</sup>*Istituto dei Sistemi Complessi (ISC-CNR), Via dei Taurini 19, I-00185 Rome, Italy* (Received 20 May 2024; revised 19 June 2024; accepted 24 June 2024; published 11 July 2024)

The iron-based superconductor FeSe isovalently substituted with S displays an abundance of remarkable phenomena that have not been fully understood, at the center of which are apparent zero-energy excitations in the superconducting state in the tetragonal phase. The phenomenology has been generally consistent with the proposal of the so-called ultranodal states where Bogoliubov Fermi surfaces (BFSs) are present. Recently, nuclear magnetic resonance measurements have seen unusually large upturns in the relaxation rate as temperature decreases to nearly zero in these systems, calling for theoretical investigations. In this paper, we calculate the spin susceptibility of an ultranodal superconductor including correlation effects within the random phase approximation. Although the noninteracting mean-field calculation rarely gives an upturn in the low-temperature relaxation rate within our model, we found that correlation strongly enhances scattering between coherent parts of the BFS, resulting in robust upturns when the interaction is strong. Our results suggest that, in addition to the presence of BFSs, correlation and multiband physics also play important roles in the low-energy excitations of the system.

DOI: [10.1103/PhysRevB.110.L020503](https://doi.org/10.1103/PhysRevB.110.L020503)

**Introduction.** Iron-based superconductors have been drawing lots of research interest for almost two decades since their discovery, for their relatively high  $T_c$ , simple structure, and the interplay between rich phenomena including nematicity, magnetization, and nontrivial topology [1]. Among all families of iron-based superconductors, the chalcogenide 11 material FeSe has a distinct phase diagram where a nematic transition can occur without accompanying magnetic order [2–7]. The parent compound FeSe shows a nematic transition at  $\sim 90$  K, a superconducting (SC) transition at 9 K, and no magnetic order under ambient pressure. Upon applying hydrostatic pressure, the nematicity is suppressed, and antiferromagnetic (AFM) order develops. The AFM order in FeSe under pressure should resemble that observed in iron pnictides and is likely a stripe order with in-plane magnetic moments [1,8–10].

On the other hand, S-substituted FeSe does not show strong evidence for long-ranged magnetic order but exhibits peculiar changes in its SC states across the nematic quantum critical point (QCP) at  $\sim 0.17$  sulfur substitution. For  $x > 0.17$ , the normal state of FeSe<sub>1-x</sub>S<sub>x</sub> is tetragonal, established by various measurements of the electronic structure [2,11,12], and the transport properties show non-Fermi liquid behavior near the QCP [13]. The SC state shows curiously large zero-energy density of states (DOS), which has so far been evidenced by specific heat and thermal transport measurements [14], scanning tunneling microscopy (STM) [15], angular-resolved photoemission spectroscopy (ARPES) [16], and most recently, by nuclear magnetic resonance (NMR) studies [17].

Possible origins of such residual DOS in the SC states of the heavily S-substituted FeSe has been discussed in Refs. [16,17]. Impurity effects or coexistence of spatially separated SC and normal phases are excluded because the samples are clean and homogeneous, as seen from quantum oscillation [2] and STM experiments [15]. For measurements done under external field such as the NMR measurements, another possible explanation for the observed residual DOS is the Volovik effect [18,19]. However, the Volovik effect cannot account for the order of magnitude difference in the relaxation rate across samples with different substitution levels but the same external field. It has been suggested [20–22] that the so-called ultranodal SC state, which by definition hosts Bogoliubov Fermi surfaces (BFSs), is responsible for the large residual DOS in these systems.

Ultranodal states are SC states with extended gap nodes that, in contrast with usual point nodes or line nodes in three dimensions, have the same dimension as the underlying normal state Fermi surface. Such extended nodes are called BFSs [23–28]. The existence of BFSs does not necessarily require nontrivial topology, as is the case in Ref. [29], but they are topologically protected by a  $\mathbb{Z}_2$  invariant if the SC state possesses inversion symmetry. In a multiband spin- $\frac{1}{2}$  superconductor, BFSs can arise from an interband nonunitary triplet pairing term or from a magnetic order that breaks time-reversal symmetry and may [20] or may not [22,29] preserve the inversion symmetry. It has also been shown [22] that the nonunitarity of the interband triplet pairing can be induced by driving the system close to a magnetic instability, in which case the magnetic moment of the nonunitary triplet pair aligns with the fluctuating magnetic order.

\*Contact author: yifucao@ufl.edu

The existence of a BFS explains well the residual DOS in the tetragonal Fe(Se,S), as seen from specific heat or STS experiments (see, however, Ref. [30] for an alternative picture) as well as the possible  $C_4$  symmetry breaking in the SC phase, as seen in the ARPES experiment [16]. However, it has not been fully understood how the ultranodal scenario can fit the recent NMR data presented in Ref. [17].

The NMR measurements in Ref. [17], performed on FeSe<sub>1-x</sub>S<sub>x</sub> at several S-substitution levels across the nematic QCP with in-plane applied field and temperature down to 100 mK, show not only finite values of  $1/(T_1 T)$  at zero temperature for the  $x = 0.18$  and  $0.23$  samples but also unusual upturns as temperature decreases toward zero. While the former can be understood fairly straightforwardly as yet another signature of the zero-energy residual DOS in these materials, the latter requires a more sophisticated understanding. In this letter, we study the models for BFS systems discussed in Refs. [20–22] to further calculate the spin fluctuations in the ultranodal states. We compare our calculations of  $1/(T_1 T)$  to the experimental data and show that the upturn is likely due to the interplay between strong magnetic fluctuation and multiband physics in such systems.

*Model.* To obtain BFSs with relevance for the Fe(Se,S) system, we rely on the electronic structure having two hole pockets (or incipient hole pockets) with small splitting at the  $\Gamma$  point. The electron pockets at the  $X$  and  $Y$  points are not relevant for the low-temperature upturn in  $1/(T_1 T)$  driven by the existence of BFSs since we expect that any reasonable interband pairing strength involving the electron bands would not be strong enough to create BFSs near the electron pockets. Therefore, we consider a minimal two-band mean field model, corresponding to the two hole bands at the  $\Gamma$  point, with intra-band spin-singlet pairing and interband nonunitary spin-triplet pairing adopted from previous works [20–22]:

$$H = \sum_{\mathbf{k}, \sigma, i} \epsilon_{i\mathbf{k}\sigma} c_{i\mathbf{k}\sigma}^\dagger c_{i\mathbf{k}\sigma} - \sum_{\mathbf{k}, i} \Delta_i(\mathbf{k})(c_{i\mathbf{k}\uparrow}^\dagger c_{i-\mathbf{k}\downarrow}^\dagger + \text{H.c.}) - \sum_{\mathbf{k}, \sigma} \Delta_{\sigma\sigma}(\mathbf{k})(c_{1\mathbf{k}\sigma}^\dagger c_{2-\mathbf{k}\sigma}^\dagger + \text{H.c.}). \quad (1)$$

Here,  $i = 1, 2$  is the band index. Seeking qualitative results at low temperatures, we make the assumption that all gaps correspond to a single  $T_c$  and follow a BCS-like temperature dependence, where the key feature is that the deviation from the  $T = 0$  value is exponentially or power-law small at low temperature. Also, for simplicity, we consider a tight-binding model with only nearest-neighbor hopping and  $\epsilon_{i\mathbf{k}\sigma} = 2(\cos k_x + \cos k_y) - \mu_i$ . We have set the nearest-neighbor hopping parameter  $t = 1$  and adopt it as our unit of energy throughout the calculations below.

We calculate the spin susceptibility:

$$\chi^{uv}(\mathbf{q}, t) = i\theta(t) \sum_{\mathbf{q}'} \langle [S^u(\mathbf{q}, t), S^v(\mathbf{q}', 0)] \rangle, \quad (2)$$

where  $S^u(\mathbf{q}, t = 0) = \sum_{i, \mathbf{k}, \alpha, \beta} c_{i\mathbf{k}\alpha}^\dagger \sigma_{\alpha\beta}^u c_{i\mathbf{k}+\mathbf{q}\beta}$  is the total spin operator summed over the two bands, and  $u, v = x, y, z$ . The spin-quantization axis ( $z$  axis of the Pauli matrices) denotes the direction of the magnetic moment of our nonunitary triplet pair [22], which breaks the spin-rotational symmetry of the

ultranodal state and makes the  $z$  direction inequivalent to the  $x, y$  directions. Depending on the angle between the  $z$  direction and the applied magnetic field, all components of  $\chi^{uv}$  might contribute to the longitudinal relaxation time  $T_1$  [31]. We focus on two configurations: The external field  $\vec{B}$  is either parallel or perpendicular to the  $\hat{z}$  direction when calculating  $T_1$ , and all the other configurations should give results in between these two configurations. For  $\vec{B} \parallel \hat{z}$ ,

$$\frac{1}{T_1} \propto T \lim_{\omega \rightarrow 0} \sum_{\mathbf{q}} \frac{\text{Im} \chi^{+/-}(\mathbf{q}, \omega)}{\omega}, \quad (3)$$

where  $+/-$  denotes  $x \pm iy$ . Similarly, for  $\vec{B} \parallel \hat{x}$ , Eq. (3) is still valid, except  $+/-$  now denotes  $y \pm iz$ .

To this end, we first find the Nambu Green's function  $G_{\mathbf{k}}(\omega)$  by diagonalizing the Nambu Hamiltonian corresponding to Eq. (1). The Nambu basis we use is  $\psi_{\mathbf{k}} = [c_{1\mathbf{k}\uparrow}, c_{1-\mathbf{k}\downarrow}, c_{2-\mathbf{k}\uparrow}, c_{2\mathbf{k}\downarrow}, c_{1\mathbf{k}\uparrow}^\dagger, c_{1-\mathbf{k}\downarrow}^\dagger, c_{2-\mathbf{k}\uparrow}^\dagger, c_{2\mathbf{k}\downarrow}^\dagger]^T$ . With the eigenvalues  $E_{l\mathbf{k}}$  and the eigenvector matrix  $U_{\mathbf{k}}$  of the Nambu Hamiltonian, the Nambu Green's function can be expressed as

$$G_{\mathbf{k}}(\omega) = U_{\mathbf{k}}^\dagger \text{diag} \left( \frac{1}{\omega - E_{1\mathbf{k}}}, \dots, \frac{1}{\omega - E_{8\mathbf{k}}} \right) U_{\mathbf{k}}. \quad (4)$$

At this point, we would like to also define the  $8 \times 8$  Nambu spin matrices  $\Sigma^u \equiv \text{diag}[\sigma^u, \sigma^u, -(\sigma^u)^T, -(\sigma^u)^T]$ , composed of  $2 \times 2$  Pauli matrices on their diagonal blocks. The bare spin-spin correlation function in the Matsubara representation is  $C^{uv}(\mathbf{q}, i\nu_m) = -\frac{1}{\beta} \sum_{i\omega_n} \sum_{\mathbf{k}} \text{Tr}[\Sigma^u G_{\mathbf{k}+\mathbf{q}}(i\omega_n + i\nu_m) \Sigma^v G_{\mathbf{k}}(i\omega_n)]$ , where  $\nu_m$  is a bosonic frequency. Substituting in Eq. (4) and performing the Matsubara sum and the analytic continuation to the real axis, we obtain first the bare density-density bubble in the quasiparticle band space:

$$\chi_{ll'mm'}^{(0)}(\mathbf{q}, \omega) = - \sum_{\mathbf{k}, r, s} U_{r\mathbf{k}} U_{s\mathbf{k}+\mathbf{q}}^* U_{r\mathbf{k}}^* U_{s\mathbf{k}+\mathbf{q}} \times \frac{f(E_{s\mathbf{k}+\mathbf{q}}) - f(E_{r\mathbf{k}})}{E_{s\mathbf{k}+\mathbf{q}} - E_{r\mathbf{k}} - \omega - i0^+}. \quad (5)$$

Then the  $zz$  component of the spin susceptibility can be written as

$$\chi^{(0)zz}(\mathbf{q}, \omega) = \frac{1}{2} \sum_{l, m} \Sigma_{ll}^z \Sigma_{mm}^z \chi_{llmm}^{(0)}(\mathbf{q}, \omega), \quad (6)$$

and for the other components  $u, v = x, y$ , we have

$$\chi^{(0)uv}(\mathbf{q}, \omega) = \frac{1}{2} \sum_{l, m} \Sigma_{ll}^u \Sigma_{mm}^v \chi_{llmm}^{(0)}(\mathbf{q}, \omega), \quad (7)$$

where  $\bar{l}$  denotes the Nambu index that corresponds to the time-reversed  $l$ th operator in the Nambu basis. For example,  $\bar{1} = 2$  and  $\bar{8} = 7$ . From Eqs. (6) and (7), we see that two types of  $\chi_{ll'mm'}^{(0)}$  are particularly important, namely, the  $llmm$  and  $\bar{l}\bar{l}\bar{m}\bar{m}$  types. Accordingly, let us define two types of coherence factors:

$$W_{ll}(r\mathbf{k}, s\mathbf{k}') \equiv U_{r\mathbf{k}} U_{s\mathbf{k}'}^*, \quad (8)$$

$$W_{\bar{l}\bar{l}}(r\mathbf{k}, s\mathbf{k}') \equiv U_{r\mathbf{k}} U_{s\mathbf{k}'}^*, \quad (9)$$

where  $r\mathbf{k}$  is a composite label referring to the Bogoliubov quasiparticle at momentum  $\mathbf{k}$  in the  $r$ th quasiparticle band.

They will be useful when we analyze the structure of the BFSs later.

We can further investigate using a random phase approximation (RPA) the effect of a residual interaction in the particle-hole channel. We consider an interaction of the Hubbard type:

$$H_U = \frac{1}{2} \sum_{\mathbf{r},i} U n_{i\uparrow} n_{i\downarrow} \\ = \frac{1}{16} \sum_{\mathbf{k},\mathbf{k}',\mathbf{q}} \sum_{l,m,l',m'} \Gamma_{ll'mm'} \psi_{l\mathbf{k}}^\dagger \psi_{l'\mathbf{k}-\mathbf{q}} \psi_{m'\mathbf{k}'}^\dagger \psi_{m\mathbf{k}'+\mathbf{q}}. \quad (10)$$

In the last step, we have rewritten the interaction using the Nambu basis and defined a coupling tensor  $\Gamma$  that does not depend on the momentum transfer  $\mathbf{q}$ . The nonzero elements of  $\Gamma$  are  $\Gamma_{ll\bar{l}\bar{l}} = U$  and  $\Gamma_{l\bar{l}l\bar{l}} = -U$  for  $l = 1, 2, \dots, 8$ . As shown in the Supplemental Material [32], it is sufficient to consider only the  $8 \times 8$   $llmm$  matrix blocks (with  $ll$  being the row index and  $mm$  being the column index) of  $\chi_{ll'mm'}^{(0)}$  and  $\Gamma_{ll'mm'}$ , which we denote as  $\hat{\chi}^{(0)}$  and  $\hat{\Gamma}$ , for calculating  $\chi^{(\text{RPA})zz}$ . For  $\chi^{(\text{RPA})uv}$  with  $u, v = x, y$ , it is sufficient to consider only the  $8 \times 8$   $l\bar{l}m\bar{m}$  blocks of  $\chi_{l\bar{l}m\bar{m}'}^{(0)}$  and  $\Gamma_{l\bar{l}m\bar{m}'}$ , which we denote as  $\tilde{\chi}^{(0)}$  and  $\tilde{\Gamma}$ . The RPA density-density bubble is related to the bare bubble through

$$\hat{\chi}^{(\text{RPA})}(\mathbf{q}, \omega) = \hat{\chi}^{(0)}(\mathbf{q}, \omega) [\hat{I} + \hat{\Gamma} \hat{\chi}^{(0)}(\mathbf{q}, \omega)]^{-1}; \quad (11)$$

$$\tilde{\chi}^{(\text{RPA})}(\mathbf{q}, \omega) = \tilde{\chi}^{(0)}(\mathbf{q}, \omega) [\tilde{I} + \tilde{\Gamma} \tilde{\chi}^{(0)}(\mathbf{q}, \omega)]^{-1}. \quad (12)$$

The sign convention for the above equation is also explained in detail in the Supplemental Material [32]. Here, we note only that the usual RPA sign emerges in the more standard spin basis. The RPA spin susceptibility is

$$\chi^{(\text{RPA})zz}(\mathbf{q}, \omega) = \frac{1}{2} \sum_{l,m} \Sigma_{ll}^z \Sigma_{mm}^z \hat{\chi}_{llmm}^{(\text{RPA})}(\mathbf{q}, \omega), \quad (13)$$

$$\chi^{(\text{RPA})uv}(\mathbf{q}, \omega) = \frac{1}{2} \sum_{l,m} \Sigma_{ll}^u \Sigma_{mm}^v \tilde{\chi}_{l\bar{l}m\bar{m}}^{(\text{RPA})}(\mathbf{q}, \omega), \quad (14)$$

$u, v = x, y$

by analogy to Eqs. (6) and (7) with  $\chi^{(0)} \rightarrow \hat{\chi}^{(\text{RPA})}$  or  $\tilde{\chi}^{(\text{RPA})}$ .

**Results.** We numerically calculated the spin susceptibility of the ultranodal states for the model Hamiltonian. To summarize the result, we found that the bare susceptibility calculation always gives rise to nonzero residual  $1/(T_1 T)$  at zero temperature when BFSs are present, as expected due to the zero-energy residual DOS. However, the bare  $1/(T_1 T)$  rarely increases as temperature decreases near  $T = 0$ , unless van Hove singularities of the Bogoliubov quasiparticle bands are tuned to the Fermi level, contributing to a large zero-energy peak in the DOS. On the other hand, if we consider the correlation effects using the RPA calculation, certain scattering between coherent spots/segments on the BFSs can get strongly enhanced, resulting in an upturn in  $1/(T_1 T)$  as temperature decreases, even when the zero-energy DOS is not peaked or when the BFSs are not strongly nested. Below, we discuss in detail these results.

In Figs. 1 and 2, we show in parallel two examples of having upturns in  $1/(T_1 T)$  at low temperature as a result of correlations, the existence of BFSs, and multiband effects

combined. Figure 1 corresponds to a scenario where the intraband singlet  $\Delta_i(\mathbf{k})$  is taken to be a nodal  $s$  wave with accidental nodes along the  $45^\circ$  directions, and the interband triplet pairing  $\Delta_{\uparrow\uparrow}(\mathbf{k})$  is isotropic. Figure 2 corresponds to the  $C_2$  symmetric scenario discussed in Ref. [22], where the interband triplet pairing  $\Delta_{\uparrow\uparrow}(\mathbf{k})$  is assumed to be a  $p$  wave, and the intraband singlet pairing  $\Delta_i(\mathbf{k})$  is taken to be isotropic for simplicity. A BFS then forms only when  $\Delta_{\uparrow\uparrow}$  is sufficiently large.

In both cases, we have set  $\Delta_{\downarrow\downarrow}(\mathbf{k}) = 0$ . In Fig. 1, the bare susceptibility already gives rise to upturns in the  $1/(T_1 T)$  [panels (c) and (d) cyan curve, each corresponds to different orientations of the external field]. This is because the van Hove singularity (band extremum corresponding to where the SC gap opens) of the Bogoliubov band has been tuned at the Fermi level by changing the interband order parameter, and a peak in the quasiparticle DOS exists at exactly zero energy [Fig. 1(a)]. We found that upturns in the bare  $1/(T_1 T)$  at low temperature seem to always be associated with such peaks at zero energy in the DOS. Although such peaks in the DOS are not desired, as they are fine-tuned and not consistent with the spectroscopic data [15], they are not required once we include correlations. This can be seen in Figs. 2(a)–2(d), where the DOS is not peaked at zero energy, and the bare  $1/(T_1 T)$  curve does not have an upturn, while the RPA curve close to magnetic instability does. The qualitative difference between the  $U = 0$  curve and the  $U \lesssim U_c(0)$  curve in Figs. 2(c) and 2(d) is unusual since normally one would expect, from its simplest form for the normal metal as in Eq. (S.22) in the Supplemental Material [32], the RPA susceptibility to be enhanced further where the bare susceptibility is already large.

To better understand this unusual behavior, we analyze here the major contribution to the upturns in Figs. 1(c) and 2(c) from  $\chi^{zz}$  (blue shaded area) and provide in the Supplemental Material [32] the same analysis for the contributions from  $\chi^{yy} = \chi^{xx}$  [pink or yellow shaded area in panel (c) or (d)]. We first divide the BFSs into several segments, as shown by the color scheme in Figs. 1(b) and 2(b); within each color, the scattering that preserves the spin and band is much stronger than across different colors. This is done by treating the  $\mathbf{k}$  points on the BFS as vertices of weighted undirected graphs with weights given by linear combinations of the eight  $ll$ -type coherence factors  $W_{ll}$  defined in Eq. (8) and employing the Leiden algorithm for community detection [33,34]. We see that the parts of the BFS that follow the shape of the normal Fermi surfaces [red and blue in Figs. 1(b) and 2(b)] are well separated from the rest of the BFSs in terms of non-spin-flip scattering processes. By examining the eigenvectors, we confirm that the red (blue) BFSs are mainly of the inner (outer) band character and have relatively small intraband spin-singlet particle-hole mixing, while the green BFSs feature significant interband spin-triplet particle-hole mixing and moderate intraband spin-singlet particle-hole mixing. Then in Figs. 1(e), 1(f) and 2(e), 2(f), we plot the  $zz$  component of the bare spin susceptibility as in Eq. (6) at zero temperature, and in panels (g) and (h) we show the RPA spin susceptibility in Eq. (13) at  $U \lesssim U_c(0)$  and zero temperature. We identify the important  $\mathbf{q}$  vectors as the red and green arrows connecting segments of BFSs with the same color shown in Figs. 1(b) and 2(b). From panel (e), we first see that the real part of the bare

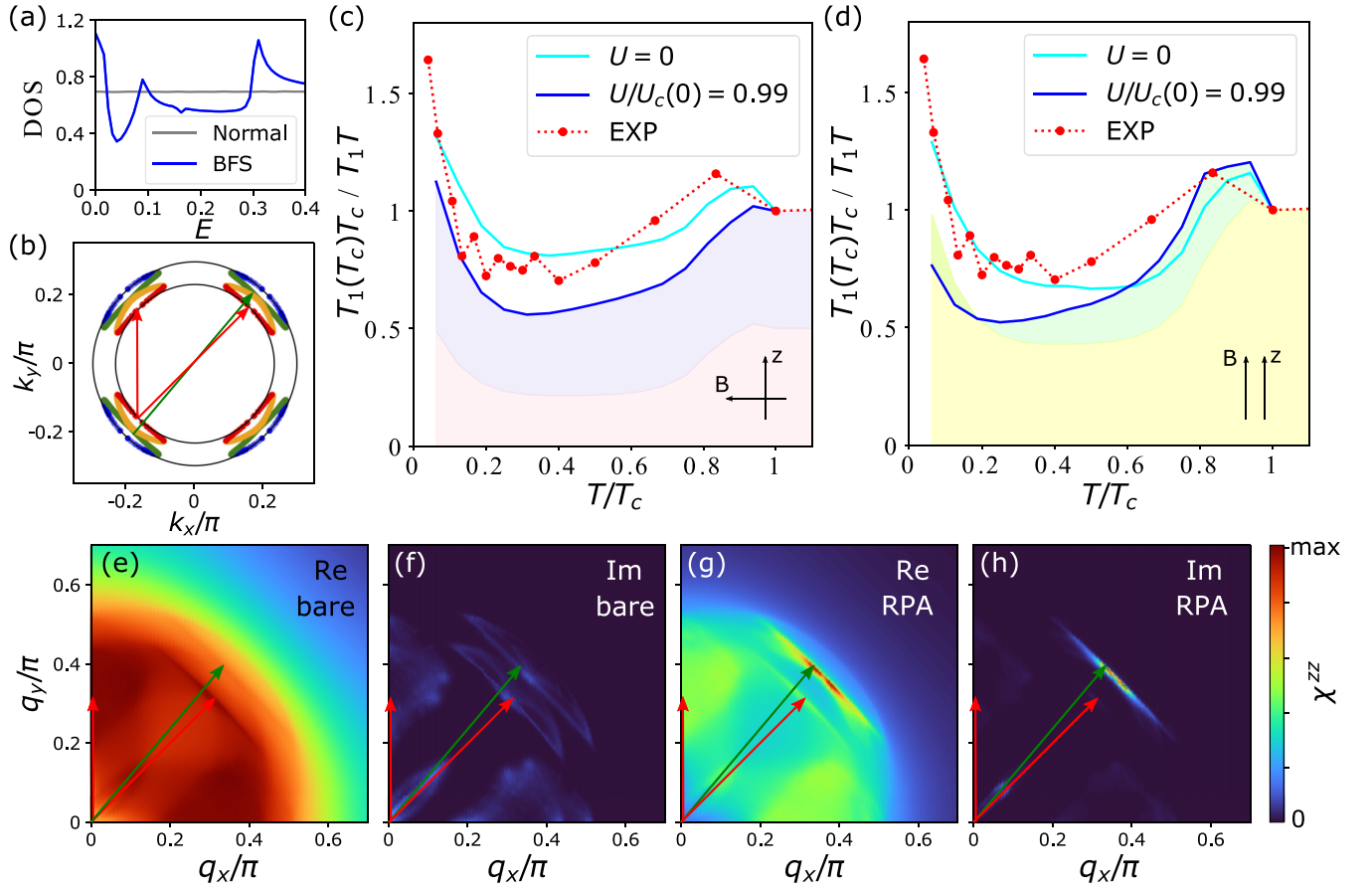


FIG. 1. (a) Zero temperature density of states (DOS) for the two-band model in Eq. (1), with  $\mu_1 = 3.5$ ,  $\mu_2 = 3.2$ , and  $\Delta_1(\mathbf{k}) = \Delta_2(\mathbf{k}) = 0.06|\cos 2\theta_{\mathbf{k}}|$ , where  $\theta_{\mathbf{k}}$  is the angle of  $\mathbf{k}$  on the two-dimensional (2D) Fermi surface.  $\Delta_{\uparrow\uparrow}(\mathbf{k}) = 0.15$ ,  $\Delta_{\downarrow\downarrow}(\mathbf{k}) = 0$  at  $T = 0$ . (b) Normal (black) and Bogoliubov (colored) Fermi surfaces. Within the same color of the Bogoliubov Fermi surface (BFS) the coherent scattering amplitudes are larger than between points on BFSs with different color (see main text Sec. III). Arrows show some of the dominant scattering processes as seen from panels (e)–(h). (c) Normalized  $1/(T_1 T)$  below  $T_c$  assuming  $\hat{z}$  perpendicular to the applied magnetic field. Cyan and blue curves calculated from bare and random phase approximation (RPA) susceptibility near a magnetic instability, respectively. Red dots are experimental data taken from Ref. [17]. The pink and blue shaded areas represent contributions from  $\text{Im } \chi^{yy}$  and  $\text{Im } \chi^{zz}$ , respectively.  $T_c$  is taken to be 0.08. The critical  $U$ , defined as the lowest  $U$  where any of the RPA susceptibility  $\tilde{\chi}_{l'l'mm'}^{(\text{RPA})}(\mathbf{q}, \omega)$  component diverges for any  $\mathbf{q}$  vector, is determined from the normal and Bogoliubov band structure, and  $U_c(T_c) = 10.8$ ,  $U_c(0) = 9.6$ . (d) Normalized  $1/(T_1 T)$  below  $T_c$  assuming  $\hat{z}$  parallel to the applied magnetic field. The yellow and green shaded areas represent contributions from  $\text{Im}(\chi^{xx} + \chi^{yy})$  and  $\text{Re } \chi^{yy}$ , respectively. Note that the contribution from  $\text{Re } \chi^{yy}$  at low  $T$  is negative. (e)–(h) Real and imaginary parts of the spin susceptibility at  $T = 0$ . The arrows are the same as in (a). One can see that there is a shift of the dominant contribution from the red arrow to green arrow as  $U$  increases. The color bar maxima are 0.7, 0.03, 8.5, and 9 for (e)–(h), respectively.

susceptibility is the largest at the  $\mathbf{q}$  vectors connecting the red part of the BFSs but is not strongly peaked at any particular  $\mathbf{q}$  vector. The latter observation is an indication of no strong nesting between the the BFSs. Secondly, by comparing panels (e) and (f) with panels (g) and (h) in Figs. 1 and 2, we see that, although the  $\mathbf{q}$  vectors that connect the green part of the BFSs are only subdominant in the bare susceptibility, they become the dominant  $\mathbf{q}$  vectors near the magnetic instability. This shift of the dominant  $\mathbf{q}$  vectors as the interaction  $U$  increases within an RPA calculation can only be explained by nontrivial multiband effects embedded in the coherence factor  $W_{ll}$ , which is consistent with the unusual change in the shape of the normalized  $1/(T_1 T)$  curve as  $U$  increases. Since this multiband effect can be seen in both the  $C_4$  and  $C_2$  examples as from Figs. 1 and 2, we claim that, although the parameter set we chose to demonstrate the effects of fine-tuning

corresponded to a  $C_4$  symmetric BFS, the upturn in  $1/(T_1 T)$  from the RPA calculations should be generically present in both  $C_4$  and  $C_2$  cases irrespective of rotational symmetry without fine-tuning.

In case the external field fully polarizes the magnetic moment of the nonunitary triplet pair so that  $\vec{B} \parallel \hat{z}$ ,  $\chi^{zz}$  will not be responsible for the longitudinal relaxation at all. Nevertheless, as seen in Figs. 1(d) and 2(d), there will still be a minor upturn in  $1/(T_1 T)$  due to contributions from  $\chi^{xx} = \chi^{yy}$ . They share some key features with  $\chi^{zz}$ , as discussed in the previous paragraph (see Supplemental Material [32]): First, there can be shifts of the dominant  $\mathbf{q}$  vector as  $U$  increases. Second, only those  $\mathbf{q}$  vectors connecting coherent parts of the BFS, which usually carry interband character, contribute significantly to the susceptibility at  $T = 0$ . Therefore, the low-temperature upturns in Figs. 1(d) and 2(d) have the same origin as in panel

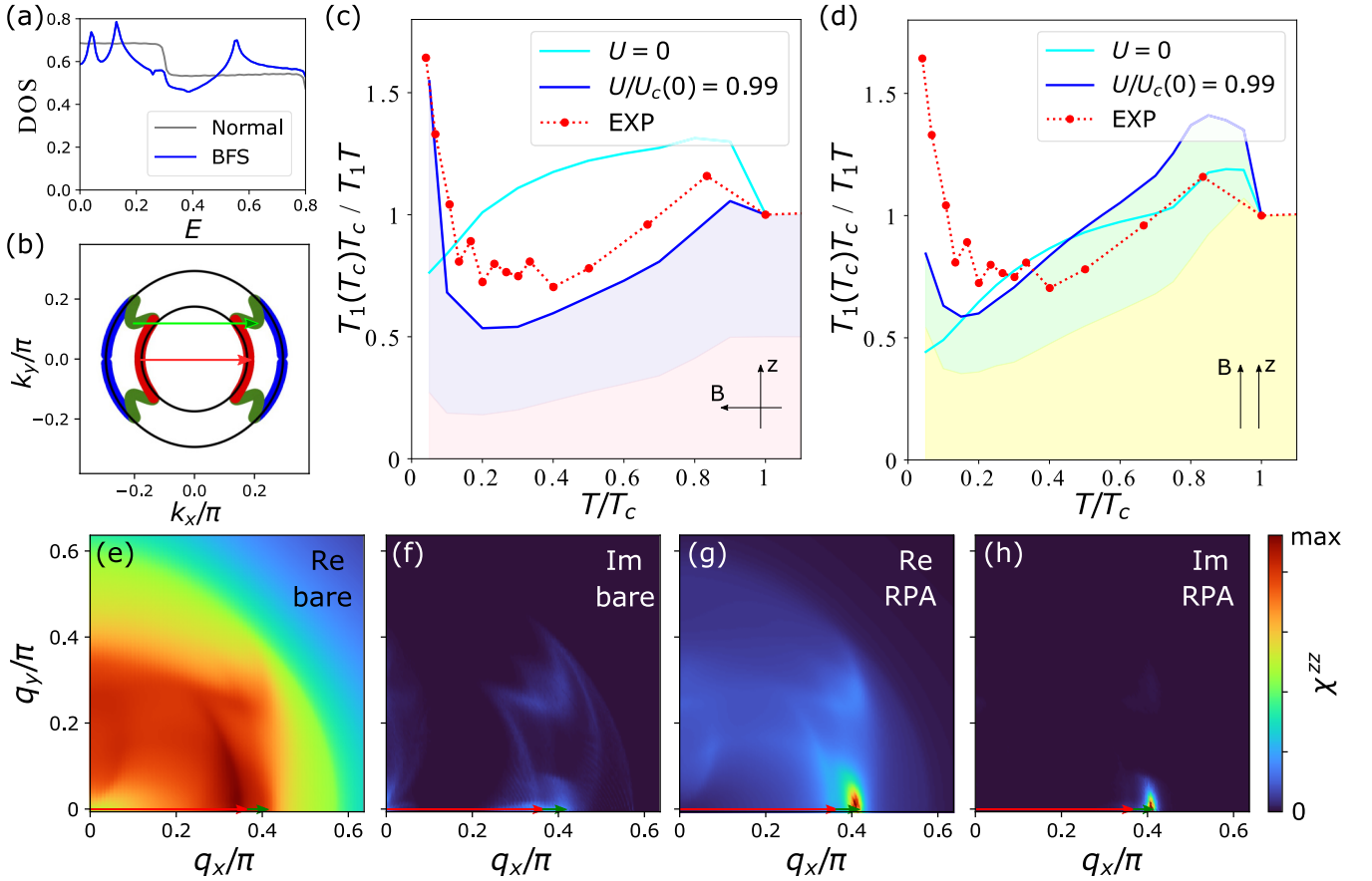


FIG. 2. Same as Fig. 1 but with a different set of parameters:  $\mu_1 = 3.7$ ,  $\mu_2 = 3.2$ ,  $\Delta_1(\mathbf{k}) = \Delta_2(\mathbf{k}) = 0.05$ ,  $\Delta_{\uparrow\uparrow}(\mathbf{k}) = 0.3 \cos \theta_{\mathbf{k}}$ ,  $\Delta_{\downarrow\downarrow}(\mathbf{k}) = 0$ ,  $T_c = 0.1$ ,  $U_c(T_c) = 10.8$ , and  $U_c(0) = 10.1$ . The color bar maxima are 0.7, 0.026, 35, and 11 for (e)–(h), respectively.

(c), namely, it is due to the existence of BFSs, correlation, and multiband physics.

**Conclusions.** To summarize, we have calculated the spin susceptibilities for the ultranodal states in a minimal two-band model, where the interband nonunitary spin-triplet pairing is responsible for the BFSs. We found that the existence of BFSs in such models naturally gives rise to finite residual value in  $1/(T_1T)$  at zero temperature but does not necessarily produce the large upturns at low temperature, as seen in the experiments [17] on the Fe(Se,S) system, in a noninteracting calculation. We then studied the effect of correlations within RPA in the ultranodal state. By adding a Hubbard interaction in the particle-hole channel while not changing the presumed pairing gaps, we see that the spin susceptibilities at  $\mathbf{q}$  vectors connecting coherent segments/spots on the BFS get strongly enhanced at low temperature when the interaction is strong, resulting in upturns in  $1/(T_1T)$  irrespective of the presence or absence of upturns in the bare calculation. These spots have strong interband character, as indicated from their position on the BFSs, and do not have particularly large contribution to the spin susceptibilities at weak interaction. The  $1/(T_1T)$  calculated from the spin susceptibilities close to the AFM instability shows robust upturns at low temperature for all orientations of external field. Although the upturn is the smallest when the Cooper pair moment aligns with the

external field, we expect that spin-orbit coupling or strong AFM fluctuations could drive the system away from the perfectly polarized configuration. Therefore, we conclude that the experimentally observed upturn in  $1/(T_1T)$  can be explained as a combined effect of the presence of BFSs, interband physics, and correlation.

Our theory is primarily applicable to the tetragonal phase of  $\text{FeSe}_{1-x}\text{S}_x$  with  $x > 0.17$  at ambient pressure. For the nematic phase with  $x < 0.17$  at ambient pressure and the tetragonal phase with  $x < 0.17$  under pressure [35], the low-temperature  $1/(T_1T)$  seems to have a Korringa behavior, i.e., constant in temperature, with smaller but finite residual values. Our calculation of  $1/(T_1T)$  is consistent with these data, assuming weak correlation or small BFSs, but whether the ultranodal scenario can apply to these situations requires a more careful and comprehensive study in the future.

**Acknowledgments.** L.F. acknowledges support by the European Union’s Horizon 2020 research and innovation programme through the Marie Skłodowska-Curie grant SuperCoop (Grant No. 838526). P.J.H. and Y.C. were supported by the U.S. Department of Energy Grant No. DE-FG02-05ER46236. A.K. acknowledges support by the Danish National Committee for Research Infrastructure (NUFI) through the ESS-Lighthouse Q-MAT.

- [1] R. Fernandes, A. Coldea, H. Ding, I. Fisher, P. Hirschfeld, and G. Kotliar, Iron pnictides and chalcogenides: A new paradigm for superconductivity, *Nature (London)* **601**, 35 (2022).
- [2] A. I. Coldea, S. F. Blake, S. Kasahara, A. A. Haghighirad, M. D. Watson, W. Knafo, E. S. Choi, A. McCollam, P. Reiss, T. Yamashita *et al.*, Evolution of the low-temperature fermi surface of superconducting  $\text{FeSe}_{1-x}\text{S}_x$  across a nematic phase transition, *npj Quantum Mater.* **4**, 2 (2019).
- [3] A. Kreisel, P. J. Hirschfeld, and B. M. Andersen, On the remarkable superconductivity of FeSe and its close cousins, *Symmetry* **12**, 1402 (2020).
- [4] J. Sun, K. Matsuura, G. Ye, Y. Mizukami, M. Shimozawa, K. Matsubayashi, M. Yamashita, T. Watashige, S. Kasahara, Y. Matsuda *et al.*, Dome-shaped magnetic order competing with high-temperature superconductivity at high pressures in FeSe, *Nat. Commun.* **7**, 12146 (2016).
- [5] K. Matsuura, Y. Mizukami, Y. Arai, Y. Sugimura, N. Maejima, A. Machida, T. Watanuki, T. Fukuda, T. Yajima, Z. Hiroi *et al.*, Maximizing  $T_c$  by tuning nematicity and magnetism in  $\text{FeSe}_{1-x}\text{S}_x$  superconductors, *Nat. Commun.* **8**, 1143 (2017).
- [6] M. Bendele, A. Amato, K. Conder, M. Elender, H. Keller, H.-H. Klauss, H. Luetkens, E. Pomjakushina, A. Raselli, and R. Khasanov, Pressure induced static magnetic order in superconducting  $\text{FeSe}_{1-x}$ , *Phys. Rev. Lett.* **104**, 087003 (2010).
- [7] T. Terashima, N. Kikugawa, S. Kasahara, T. Watashige, T. Shibauchi, Y. Matsuda, T. Wolf, A. E. Böhmer, F. Hardy, C. Meingast *et al.*, Pressure-induced antiferromagnetic transition and phase diagram in FeSe, *J. Phys. Soc. Jpn.* **84**, 063701 (2015).
- [8] P. S. Wang, S. S. Sun, Y. Cui, W. H. Song, T. R. Li, R. Yu, H. Lei, and W. Yu, Pressure induced stripe-order antiferromagnetism and first-order phase transition in FeSe, *Phys. Rev. Lett.* **117**, 237001 (2016).
- [9] C. de la Cruz, Q. Huang, J. W. Lynn, J. Li, W. Ratcliff, II, J. L. Zarestky, H. A. Mook, G. F. Chen, J. L. Luo, N. L. Wang *et al.*, Magnetic order close to superconductivity in the iron-based layered  $\text{LaO}_{1-x}\text{F}_x\text{FeAs}$  systems, *Nature (London)* **453**, 899 (2008).
- [10] R. Stadel, D. D. Khalyavin, P. Manuel, K. Yokoyama, S. Lapidus, M. H. Christensen, R. M. Fernandes, D. Phelan, D. Y. Chung, R. Osborn *et al.*, Multiple magnetic orders in  $\text{LaFeAs}_{1-x}\text{P}_x\text{O}$  uncover universality of iron-pnictide superconductors, *Commun. Phys.* **5**, 146 (2022).
- [11] A. I. Coldea, Electronic nematic states tuned by isoelectronic substitution in bulk  $\text{FeSe}_{1-x}\text{S}_x$ , *Front. Phys.* **8**, 594500 (2021).
- [12] P. Reiss, M. D. Watson, T. K. Kim, A. A. Haghighirad, D. N. Woodruff, M. Bruma, S. J. Clarke, and A. I. Coldea, Suppression of electronic correlations by chemical pressure from FeSe to FeS, *Phys. Rev. B* **96**, 121103(R) (2017).
- [13] S. Licciardello, J. Buhot, J. Lu, J. Ayres, S. Kasahara, Y. Matsuda, T. Shibauchi, and N. E. Hussey, Electrical resistivity across a nematic quantum critical point, *Nature (London)* **567**, 213 (2019).
- [14] Y. Sato, S. Kasahara, T. Taniguchi, X. Xing, Y. Kasahara, Y. Tokiwa, Y. Yamakawa, H. Kontani, T. Shibauchi, and Y. Matsuda, Abrupt change of the superconducting gap structure at the nematic critical point in  $\text{FeSe}_{1-x}\text{S}_x$ , *Proc. Natl. Acad. Sci. USA* **115**, 1227 (2018).
- [15] T. Hanaguri, K. Iwaya, Y. Kohsaka, T. Machida, T. Watashige, S. Kasahara, T. Shibauchi, and Y. Matsuda, Two distinct superconducting pairing states divided by the nematic end point in  $\text{FeSe}_{1-x}\text{S}_x$ , *Sci. Adv.* **4**, eaar6419 (2018).
- [16] T. Nagashima, T. Hashimoto, S. Najafzadeh, S.-i. Ouchi, T. Suzuki, A. Fukushima, S. Kasahara, K. Matsuura, M. Qiu, Y. Mizukami *et al.*, Discovery of nematic Bogoliubov Fermi surface in an iron-chalcogenide superconductor, preprint available at Research Square, <https://doi.org/10.21203/rs.3.rs-2224728/v1> (2022).
- [17] Z. Yu, K. Nakamura, K. Inomata, X. Shen, T. Mikuri, K. Matsuura, Y. Mizukami, S. Kasahara, Y. Matsuda, T. Shibauchi *et al.*, Spin fluctuations from Bogoliubov Fermi surfaces in the superconducting state of S-substituted FeSe, *Commun. Phys.* **6**, 175 (2023).
- [18] G. E. Volovik, Superconductivity with lines of gap nodes: Density of states in the vortex, *P. Zh. Eksp. Teor. Fiz.* **58**, 457 (1993) [*JETP Lett.* **58**, 469 (1993)].
- [19] Y. Bang, Volovik effect on NMR measurements of unconventional superconductors, *Phys. Rev. B* **85**, 104524 (2012).
- [20] C. Setty, S. Bhattacharyya, Y. Cao, A. Kreisel, and P. J. Hirschfeld, Topological ultranodal pair states in iron-based superconductors, *Nat. Commun.* **11**, 523 (2020).
- [21] C. Setty, Y. Cao, A. Kreisel, S. Bhattacharyya, and P. J. Hirschfeld, Bogoliubov Fermi surfaces in spin- $\frac{1}{2}$  systems: Model Hamiltonians and experimental consequences, *Phys. Rev. B* **102**, 064504 (2020).
- [22] Y. Cao, C. Setty, L. Fanfarillo, A. Kreisel, and P. J. Hirschfeld, Microscopic origin of ultranodal superconducting states in spin- $\frac{1}{2}$  systems, *Phys. Rev. B* **108**, 224506 (2023).
- [23] G. Volovik, Zeroes in the energy gap in superconductors with high transition temperature, *Phys. Lett. A* **142**, 282 (1989).
- [24] D. F. Agterberg, P. M. R. Brydon, and C. Timm, Bogoliubov Fermi surfaces in superconductors with broken time-reversal symmetry, *Phys. Rev. Lett.* **118**, 127001 (2017).
- [25] C. Timm, A. P. Schnyder, D. F. Agterberg, and P. M. R. Brydon, Inflated nodes and surface states in superconducting half-Heusler compounds, *Phys. Rev. B* **96**, 094526 (2017).
- [26] P. M. R. Brydon, D. F. Agterberg, H. Menke, and C. Timm, Bogoliubov Fermi surfaces: General theory, magnetic order, and topology, *Phys. Rev. B* **98**, 224509 (2018).
- [27] S. Sumita, T. Nomoto, K. Shiozaki, and Y. Yanase, Classification of topological crystalline superconducting nodes on high-symmetry lines: Point nodes, line nodes, and Bogoliubov Fermi surfaces, *Phys. Rev. B* **99**, 134513 (2019).
- [28] S. Autti, J. T. Mäkinen, J. Rysti, G. E. Volovik, V. V. Zavjalov, and V. B. Eltsov, Exceeding the Landau speed limit with topological Bogoliubov Fermi surfaces, *Phys. Rev. Res.* **2**, 033013 (2020).
- [29] H. Wu, A. Amin, Y. Yu, and D. F. Agterberg, Nematic Bogoliubov Fermi surfaces from magnetic toroidal order in  $\text{FeSe}_{1-x}\text{S}_x$ , *Phys. Rev. B* **109**, L220501 (2024).
- [30] K. Ranjibul Islam and A. Chubukov, Unconventional superconductivity near a nematic instability in a multi-orbital system, *npj Quantum Materials* **9**, 28 (2024).
- [31] T. Moriya, Nuclear magnetic relaxation in antiferromagnetics, *Prog. Theor. Phys.* **16**, 23 (1956).
- [32] See Supplemental Material at <http://link.aps.org/supplemental/10.1103/PhysRevB.110.L020503> for more information on RPA

- calculation and  $q$ -dependent spin susceptibility, which includes Refs. [34,36,37].
- [33] V. A. Traag, L. Waltman, and N. J. Van Eck, From Louvain to Leiden: Guaranteeing well-connected communities, *Sci. Rep.* **9**, 5233 (2019).
- [34] G. Csardi and T. Nepusz, The igraph software package for complex network research, *InterJournal Complex Systems* **1695**, 1 (2006).
- [35] K. Rana, L. Xiang, P. Wiecki, R. A. Ribeiro, G. G. Lesseux, A. E. Böhmer, S. L. Bud'ko, P. C. Canfield, and Y. Furukawa, Impact of nematicity on the relationship between antiferromagnetic fluctuations and superconductivity in  $\text{FeSe}_{0.91}\text{S}_{0.09}$  under pressure, *Phys. Rev. B* **101**, 180503(R) (2020).
- [36] A. T. Rømer, D. D. Scherer, I. M. Eremin, P. J. Hirschfeld, and B. M. Andersen, Knight shift and leading superconducting instability from spin fluctuations in  $\text{Sr}_2\text{RuO}_4$ , *Phys. Rev. Lett.* **123**, 247001 (2019).
- [37] A. T. Rømer, T. A. Maier, A. Kreisel, P. J. Hirschfeld, and B. M. Andersen, Leading superconducting instabilities in three-dimensional models for  $\text{Sr}_2\text{RuO}_4$ , *Phys. Rev. Res.* **4**, 033011 (2022).